Stability of two immiscible leaky-dielectric liquids subjected to a radial electric field in an annulus duct

Zijing Ding, Teck Neng Wong, and Haiwang Li

Citation: Physics of Fluids (1994-present) **25**, 124103 (2013); doi: 10.1063/1.4840815
View online: http://dx.doi.org/10.1063/1.4840815
View Table of Contents: http://scitation.aip.org/content/aip/journal/pof2/25/12?ver=pdfcov
Published by the AIP Publishing

PHYSICS OF FLUIDS **25**, 124103 (2013)

Stability of two immiscible leaky-dielectric liquids subjected to a radial electric field in an annulus duct

Zijing Ding,[1] Teck Neng Wong,[1,a)] and Haiwang Li[1,2]
[1]*School of Mechanical and Aerospace Engineering, Nanyang Technological University, Singapore 639798*
[2]*National Key Lab. of Science and Technology on Aero-Engines, Beijing University of Aeronautics and Astronautics, Beijing 100191, China*

(Received 7 February 2013; accepted 21 November 2013; published online 13 December 2013)

In this paper, we investigated the stability of a two coaxial leaky dielectric fluid system flowing in an annulus duct. A constant pressure gradient was applied to drive the flow in the duct. A radial electric field was imposed between the outer and inner surfaces of the duct. Linear stability analysis was employed to discuss the influences of electric field on the capillary and interface wave instabilities. The former instability is caused by surface tension and the latter is caused by viscosity stratification at the interface. It was found that, depending on the electrical permittivities and conductivities of the two liquids, the electric field either stabilized or destabilized the flow system. Apart from that, it was found that an external electric field could impede the capillary and interface wave instabilities. Influences of the inner radius of the duct, viscosity ratio, thickness ratio, and Reynolds number on the stability of the system were discussed as well. © *2013 AIP Publishing LLC*. [http://dx.doi.org/10.1063/1.4840815]

I. INTRODUCTION

Electrohydrodynamics (EHD) studies the relation between the electric field and fluid motion. Generally, there are two branches of this subject, depending on the strength of electric field. One deals with weak electric field that is induced by free ions in electrolytes;[1,2] while the other deals with strong electric field, considering the liquids as perfect conductors,[3–5] perfect dielectrics or leaky dielectrics.

As early as 1960s, Taylor[6] realized that even a small conductivity in the liquid can allow charge to accumulate at fluid interface; and he introduced the leaky dielectric model. The leaky dielectric model assumes that there is no free charge in the bulk fluid. Therefore, no body force is present in the fluids. Electrical force only appears on the fluid surface. The interfacial instabilities of leaky dielectric fluids subjected to tangential and normal electric fields were respectively studied by Melcher and Schwarz,[7] and Melcher and Smith.[8] A detailed review of the leaky dielectric model proposed by Taylor and Melcher was provided by Saville.[9]

In industrial application, EHD is widely encountered. One of the most important applications is the mixing problem in micro-fluidics.[10,11] In microscale flows, the Reynolds number *Re* is often smaller than unity. Thus, the flow is laminar and mixing due to turbulence will not occur. Apart from that, droplet formation in immiscible fluids is another important problem in micro-fluidics which attracts the attention of many scientists. The droplet formation is due to interfacial instability and its size is determined by the wave number of the most unstable perturbation. Ozen *et al.*[12] reported that the size of a droplet may be changed by altering the strength of the electric field. It is noted that in these previous studies of instability of leaky dielectric fluid, the flow system can be generally classified into two categories according to the geometry of the flow system. One is the planar flow system, while the other is the cylindrical flow system.

a)Author to whom correspondence should be addressed. Electronic mail: mtnwong@ntu.edu.sg

Abdella and Rasmussen[13] investigated the instability of plane Couette flow of two unbounded superposed fluids in a normal electric field. Results of linear stability analysis showed that the instability associated with electric field was characterized by the conductivity ratio between the two liquids. Long-wave stability of two stationary superposed immiscible leaky dielectric liquids between two parallel plates was investigated by Shankar and Sharma[14] by deriving an asymptotic model. Ozen *et al.*[15] further extended the model[14] to a pressure-driven flow system. Ozen *et al.*[15] found that the electric field either stabilized or destabilized the system depending on the electrical properties between the two liquids. Li *et al.*[16] further studied the instability of the flow system at large Reynolds number; but unlike the work of Ozen *et al.*,[15] the electric time was assumed to be far less than the fluid time.

The effect of electric field on the capillary instability of a liquid jet or liquid bridge is of particular interest and received many investigations.[17–19] Various experimental and theoretical work was done on liquid jets in the past. The earliest detailed work of a liquid jet breaking into droplets was done by Lord Rayleigh.[20] Burcham and Saville investigated the instability of liquid bridge in an applied electric field.[21] The liquid and surrounding gas were both assumed to be leaky dielectrics, and the Taylor-Melcher model was adopted. Multi-fluid systems, such as the core-annular system, studies the coupling effects between two immiscible liquids and has a wide application, for instance, in ink-jet and drug delivering. Li *et al.*[22] investigated the temporal instability of a two-coaxial liquid jet surrounded by perfect dielectric gases system under the influences of a radial electric field. Fluids in the core liquid cylinder was assumed to be perfect dielectrics and in annulus cylinder, they were assumed to be leaky dielectrics. The instabilities of the liquid jets were discussed theoretically and numerically. Li *et al.*[22] found that the liquid viscosity had a negligible effect on the cut-off wave number. However, the electric field significantly affects the cut-off wave number. López-Herrera *et al.*[23] investigated the instability of two coaxial fluids in a cylindrical duct. The interface was assumed to be uniformly charged.[23] Recently, this model[23] was extended by Wang[24] to a leaky dielectric thread surrounded by insulating annular fluids. Breakup of the liquid thread was studied by linear stability analysis and numerical simulation.[24] Wray *et al.*[25] studied a leaky-dielectric liquid film falling down a vertical cylinder driven by gravity. The liquid film was surrounded by leaky-dielectric gases. However, the dynamics of the gas phase was neglected.[25] The influence of a radial electric field on the interfacial stability was studied by the model equation.

In the two-fluid core-annular flow system, the interface may be unstable due to the azimuthal curvature and viscosity stratification. The former is well-known as Plateau-Rayleigh instability(capillary instability); while the latter is interface wave instability caused by a jump in viscosity across the interface. The two unstable modes were associated with the deformation of interface. The pioneer work of instability due to viscosity stratification was carried out by Yih[26] who investigated the instability of a two-layer flow between two parallel planar plates. The core annular flow system is of potential applications, such as in pumping crude oil through pipelines by using a less viscous liquid for lubrication where a stable liquid-liquid interface is required. The instability of two immiscible core-annular liquid layers in a pipe was first investigated by Joseph and co-workers[27,28] who found that, the stratification of viscosity either destabilized or stabilized the system. Selvam *et al.* extended the study and investigated the instability of miscible core-annular flows with viscosity stratification.[29] In these studies,[27–29] the inner liquid layer acts as the core while Dijkstra investigated two annular liquid layers surrounding a thin wire core in a pipe.[30] The instabilities due to capillary, viscosity stratification and viscous shearing were studied.[30] Dijkstra found that the inserted core played an important role in determining the unstable mode since it changed the velocity profile. The interface may be unstable due to interfacial instabilities (capillary and interface wave instabilities) from small to moderate Reynolds number.[30] When the Reynolds number was very large, the system may be unstable due to viscous shear.[30]

In previous studies,[23,24] the inner core layer was injected with a constant voltage that the interface was charged uniformly to produce a radial electric field. Such method produces an electric field in the outer liquid layer; while the electric field is zero within the inner layer. In the core-annular flow system,[30] a radial electric field can be imposed between the inserted thin metal wire and the outer electrode. To our knowledge, the system of a two-fluid flow in an annulus duct under the action of a radial electric field is different from those of previous studies.[23,24] The imposed electric

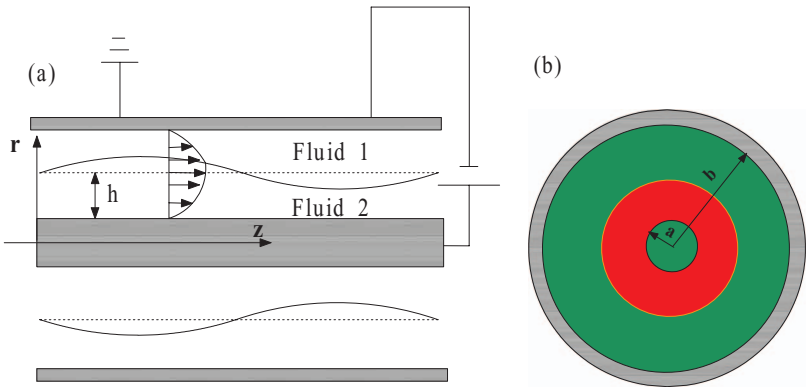

FIG. 1. Geometry of the two-fluid system. (a) Side-view. (b) Cross-section-view.

field is different from these previous studies[23,24] as well as the velocity profile. Whether the electric field can suppress the interfacial instabilities, i.e., capillary and interface wave instabilities,[30] is in question.

In this paper, we investigate a two-layer pressure-driven coaxial leaky dielectric fluid system flowing in an annulus duct, and discuss the influences of a radial external electric field on the stability of the interface. The structure of this paper is organized as follows. In Sec. II, the mathematical formation is presented. Section III gives the non-dimensional system and the base state. The linear stability analysis is carried out in Sec. IV, and the normal mode analysis is considered. Results and discussion are presented in Sec. V. A concluding remark is made in Sec. VI.

II. MATHEMATICAL FORMULATION

We consider a bilayer system as shown in Figure 1. The two liquids are considered to be leaky dielectrics and immiscible. In this paper, it is assumed that, the two-fluid system is bound by two concentric cylindrical electrodes. A constant pressure gradient is imposed in the axial direction. The outer electrode with inner radius $r = b$ is grounded, while the inner electrode with radius $r = a$ is imposed with a high electric potential. Both the liquids are considered Newtonian with constant density ρ_i, dynamical viscosity μ_i, dielectric permittivity $\varepsilon_0\varepsilon_i$ (ε_0 the vacuum electrical permittivity), electrical conductivity σ_i, where $i = 1, 2$ represents the outer layer and the inner layer respectively. Hereafter, we use $i = 1, 2$ represents the outer layer and the inner layer for simplicity, respectively.

In this paper, the two-dimensional hydrodynamical problem is considered, and the gravity is neglected. Fluids in each layer are governed by the continuity equation and the momentum equations,

$$\frac{1}{r}\frac{\partial(ru_i)}{\partial r} + \frac{\partial v_i}{\partial z} = 0, \tag{1}$$

$$\rho_i \frac{Du_i}{Dt} = -\frac{\partial p_i}{\partial r} + \mu_i(\nabla^2 u_i - \frac{u_i}{r^2}), \tag{2}$$

$$\rho_i \frac{Dv_i}{Dt} = -\frac{\partial p_i}{\partial z} + \mu_i \nabla^2 v_i, \tag{3}$$

where $(u, v)_i$ the velocity in radial and axial direction, respectively, $\frac{D}{Dt} = \frac{\partial}{\partial t} + u_i\frac{\partial}{\partial r} + v_i\frac{\partial}{\partial z}$, and $\nabla^2 = \frac{\partial^2}{\partial r^2} + \frac{1}{r}\frac{\partial}{\partial r} + \frac{\partial^2}{\partial z^2}$.

Since we are considering leaky dielectrics, the electric potential in each layer follows the solution of Laplace's equation

$$\nabla^2\phi_i = 0. \tag{4}$$

Boundary conditions on the inner surface $r = a$ are

$$u_2 = v_2 = 0, \quad \phi_2 = \phi_0. \tag{5}$$

At $r = b$, boundary conditions are expressed as

$$u_1 = v_1 = 0, \quad \phi_1 = 0. \tag{6}$$

At the liquid-liquid interface, $r = a + h(z, t)$, continuity of the velocity gives

$$u_2 = u_1, \quad v_2 = v_1. \tag{7}$$

The stress is balanced between the two liquid layer by surface tension,

$$(\mathbb{T}_2 - \mathbb{T}_1) \cdot \mathbf{n} = -\gamma(\nabla_s \cdot \mathbf{n})\mathbf{n}, \tag{8}$$

where $\mathbb{T}_i = \mathbb{T}_i^v + \mathbb{T}_i^E$ is the stress tensor. $\mathbb{T}_i^v$ stands for the viscous stress tensor and $\mathbb{T}_i^E = \varepsilon_0\varepsilon_i[\mathbf{E}_i\mathbf{E}_i - \frac{1}{2}(\mathbf{E}_i \cdot \mathbf{E}_i)\mathbb{I}]$ stands for the Maxwell stress tensor and $\mathbf{E}_i = -\nabla\phi_i$. $\mathbb{I}$ is the identity tensor. γ is the surface tension which is constant because the Marangoni effect is neglected in this paper. $\mathbf{n} = \frac{\mathbf{e}_r}{(1+h_z^2)^{\frac{1}{2}}} - \frac{h_z\mathbf{e}_z}{(1+h_z^2)^{\frac{1}{2}}}$ is the surface normal.

Continuity of electric potential at the interface gives

$$\phi_2 = \phi_1. \tag{9}$$

For leaky dielectrics, when the ratio of the fluid to electric time scales $\frac{t_E}{t_E} = \frac{h/V_I}{\varepsilon_0/\sigma}$ (V_I is the velocity scale and σ stands for the electric conductivity scale) is very large,[16] the conservative equation of interfacial charge reduces to

$$\mathbf{n} \cdot (\sigma_2\nabla\phi_2 - \sigma_1\nabla\phi_1) = 0. \tag{10}$$

Finally, we close up the system by using the kinematic equation of the liquid-liquid interface

$$h_t + v_2 h_z - u_2 = 0. \tag{11}$$

III. NON-DIMENSIONALIZATION AND BASE STATE

We introduce non-dimensional scales to non-dimensionalize the governing system (1)–(11). We use the properties of the inner layer, i.e., ρ_2, μ_2, σ_2 as the property scales, and the electrical permittivity scale is referred to vacuum permittivity ε_0. The length scale refers to the mean depth of the inner layer h_0. The velocity scale refers to the moving velocity of interface V_I at steady state, and the time scale is given by h_0/V_I. The voltage difference between the two cylinders $\Delta\phi = \phi_0 - \phi_g$($\phi_g$ is denoted as the potential of ground, $\phi_g = 0$.) is chosen as the electric potential scale. The relationship between dimensional variables and dimensionless variables (primed) is presented as follows:

$$\begin{cases} (r, z, h) = (r', z', h')h_0, \\ (u, v)_i = (u', w')_i V_I, \\ (p_1, p_2) = (p'_1, p'_2)\dfrac{\mu_2 V_I}{h_0}, \quad t = t'\dfrac{h_0}{V_I}, \\ (\phi_1 - \phi_g) = \phi'_1\Delta\phi, \quad (\phi_2 - \phi_g) = \phi'_2\Delta\phi, \\ (\mathbf{E}_1, \mathbf{E}_2) = (\mathbf{E}'_1, \mathbf{E}'_2)\dfrac{\Delta\phi}{h_0}. \end{cases} \tag{12}$$

By using these scales, after dropping the primes, the inner layer is governed by the following dimensionless equations

$$\frac{1}{r}\frac{\partial(ru_2)}{\partial r} + \frac{\partial v_2}{\partial z} = 0, \tag{13}$$

$$Re\frac{Du_2}{Dt} = -\frac{\partial p_2}{\partial r} + (\nabla^2 u_2 - \frac{u_2}{r^2}), \tag{14}$$

$$Re\frac{Dv_2}{Dt} = -\frac{\partial p_2}{\partial z} + \nabla^2 v_2, \tag{15}$$

$$\nabla^2 \phi_2 = 0, \tag{16}$$

where $Re = \frac{\rho V_I h_0}{\mu}$ is the Reynolds number.

For the outer layer, the dimensionless governing equations are

$$\frac{1}{r}\frac{\partial (ru_1)}{\partial r} + \frac{\partial v_1}{\partial z} = 0, \tag{17}$$

$$\rho Re\frac{Du_1}{Dt} = -\frac{\partial p_1}{\partial r} + \mu(\nabla^2 u_1 - \frac{u_1}{r^2}), \tag{18}$$

$$\rho Re\frac{Dv_1}{Dt} = -\frac{\partial p_1}{\partial z} + \mu\nabla^2 v_1, \tag{19}$$

$$\nabla^2 \phi_1 = 0, \tag{20}$$

where $\rho = \frac{\rho_1}{\rho_2}$ denotes the density ratio, and $\mu = \frac{\mu_1}{\mu_2}$ denotes the dynamical viscosity ratio.

The dimensionless boundary conditions at $r = a$ are

$$u_2 = v_2 = 0, \quad \phi_2 = 1. \tag{21}$$

At $r = b$, the dimensionless boundary conditions are

$$u_1 = v_1 = 0, \quad \phi_1 = 0. \tag{22}$$

On the interface $r = a + h(z, t)$, after dropping the higher term proportional to $(h_z)^2$, the tangential and normal stress balance conditions are

$$[2u_r h_z + u_z + v_r - 2v_z h_z]_2 - \mu[2u_r h_z + u_z + v_r - 2v_z h_z]_1 + We[\varepsilon_2(E_r^2 h_z + E_r E_z - E_z^2 h_z)_2 - \varepsilon_1(E_r^2 h_z + E_r E_z - E_z^2 h_z)_1] = 0, \tag{23}$$

$$-p_2 + 2[u_r - (u_z + v_r)h_z]_2 + p_1 - 2\mu[u_r - (u_z + v_r)h_z]_1 + We[\varepsilon_2(\frac{1}{2}E_r^2 - \frac{1}{2}E_z^2 - 2E_r E_z h_z)_2 - \varepsilon_1(\frac{1}{2}E_r^2 - \frac{1}{2}E_z^2 - 2E_r E_z h_z)_1] = \frac{\kappa}{Ca}, \tag{24}$$

where $We = \frac{\varepsilon_0 \Delta\phi^2}{\mu_2 V_I h_0}$ denotes the electrical Weber number, $\kappa = h_{zz} - \frac{1}{a+h}$ is the curvature. $Ca = \frac{\mu_2 V_I}{\gamma}$ is the capillary number.

The dimensionless continuity of the velocity and voltage potential conditions at the interface hold the same form as Eqs. (7) and (9),

$$u_2 = u_1, \quad v_2 = v_1, \quad \phi_2 = \phi_1, \tag{25}$$

and the dimensionless conservative law of the surface charge is

$$\mathbf{n} \cdot (\nabla\phi_2 - \sigma\nabla\phi_1) = 0, \tag{26}$$

where $\sigma = \frac{\sigma_1}{\sigma_2}$ denotes the electrical conductivity ratio.

The dimensionless kinematic condition of Eq. (11) holds the same form.

A. Base state of the system

This section deals with the base state of the flow field and electric field. The base state of the flow field and electric field are decoupled. The base velocity in radial direction vanishes and flow is parallel to the axis, i.e.,

$$\bar{u}_2 = \bar{u}_1 = 0. \tag{27}$$

Since the base state of the flow field is assumed to be uniform in z direction and driven by a constant pressure gradient along the axis, then

$$\bar{v}_2 = \frac{C}{4}r^2 + c_1 \ln(r) + c_2, \tag{28}$$

$$\bar{v}_1 = \frac{C}{4\mu}r^2 + d_1 \ln(r) + d_2, \tag{29}$$

in which

$$c_1 = \frac{C[(a+1)^2 - \mu(2a+1) - b^2]}{4(\mu \ln \frac{a+1}{a} + \ln \frac{b}{a+1})}, \tag{30}$$

$$c_2 = -\frac{C[\mu a^2 \ln \frac{a+1}{a} + a^2 \ln \frac{b}{a+1} + ((a+1)^2 - \mu(2a+1) - b^2)\ln a]}{4(\mu \ln \frac{a+1}{a} + \ln \frac{b}{a+1})}, \tag{31}$$

$$d_1 = \frac{C[(a+1)^2 - \mu(2a+1) - b^2]}{4\mu[\mu \ln \frac{a+1}{a} + \ln \frac{b}{a+1}]}, \tag{32}$$

$$d_2 = -\frac{C[((a+1)^2 - \mu(2a+1))\ln b + b^2(\mu \ln \frac{a+1}{a} - \ln(a+1))]}{4\mu[\mu \ln \frac{a+1}{a} + \ln \frac{b}{a+1}]}. \tag{33}$$

The coefficient $C = \bar{p}_z$. Since the velocity scale refers to the velocity at the interface, the dimensionless interfacial velocity $V_I = 1$. The pressure gradient is identified as

$$\frac{\partial \bar{p}}{\partial z} = \frac{4[\mu \ln \frac{a}{a+1} + \ln \frac{a+1}{b}]}{\ln \frac{a}{b} + a^2 \ln \frac{a}{a+1} + a \ln \frac{a^2}{b^2} + b^2 \ln \frac{a+1}{a}}. \tag{34}$$

The solution of the voltage potential in the inner and outer layer respectively reads

$$\bar{\phi}_2 = \frac{\sigma \ln \frac{r}{a+1} + \ln \frac{a+1}{b}}{\sigma \ln \frac{a}{a+1} + \ln \frac{a+1}{b}}, \tag{35}$$

$$\bar{\phi}_1 = \frac{\ln \frac{r}{b}}{\sigma \ln \frac{a}{a+1} + \ln \frac{a+1}{b}}. \tag{36}$$

When the inner radius is infinitely large, i.e., $a \to \infty$, the base state reduces the problem studied by Ozen *et al.*[15] as follows:

$$\bar{v}_2 = -\frac{H+\mu}{H(1+H)}y^2 + \frac{H^2+2H+\mu}{H(1+H)}y, \tag{37}$$

$$\bar{v}_1 = -\frac{H+\mu}{\mu H(1+H)}y^2 + \frac{H^2+2H+\mu}{\mu H(1+H)}y - \frac{1-\mu}{\mu}, \tag{38}$$

$$\bar{\phi}_2 = \frac{\sigma(1-y)+H}{\sigma+H}, \tag{39}$$

$$\bar{\phi}_1 = \frac{-y+H}{\sigma+H}, \tag{40}$$

where $H = b - a - 1$ represents the thickness of the outer layer, and $y = r - a$ represents the wall-normal direction. Shifting the origin to the interface, we obtain the same velocity and electric potential expressions as obtained by Ozen *et al.*[15]

IV. LINEARIZED PERTURBED SYSTEM

In this section, we study the linear stability of this system so as to provide insights on the dynamics of this system. Infinitesimal disturbances are introduced to perturb the system. In a standard way, we consider normal mode analysis. The normal mode analysis is achieved by decomposing F into $F = \bar{F}(r) + \hat{F}(r)\exp(ikz + \omega t)$, where $\bar{F}$ refers to the base state, and $\hat{F}$ the infinitesimal amplitude of a harmonic disturbance with wave number k and temporal growth rate ω. The complex temporal growth rate $\omega = \omega_r + i\omega_i$, in which, the real part ω_r is defined as the effective growth rate in this paper.

For the inner layer, the perturbed system is governed by

$$\mathtt{D}\hat{u}_2 + \frac{\hat{u}_2}{r} + ik\hat{v}_2 = 0, \tag{41}$$

$$Re\omega\hat{u}_2 = -ikRe\bar{v}_2\hat{u}_2 - \mathtt{D}\hat{p}_2 + (\mathscr{L}\hat{u}_2 - \frac{\hat{u}_2}{r^2}), \tag{42}$$

$$Re\omega\hat{v}_2 = -Re\mathtt{D}\bar{v}_2\hat{u}_2 - ikRe\bar{v}_2\hat{v}_2 - ik\hat{p}_2 + \mathscr{L}\hat{v}_2, \tag{43}$$

$$\mathscr{L}\hat{\phi}_2 = 0, \tag{44}$$

where $\mathtt{D} = \frac{d}{dr}$, $\mathscr{L} = \mathtt{D}^2 + \frac{1}{r}\mathtt{D} - k^2$.

For the outer layer, the perturbed governing system is

$$\mathtt{D}\hat{u}_1 + \frac{\hat{u}_1}{r} + ik\hat{v}_1 = 0, \tag{45}$$

$$\rho Re\omega\hat{u}_1 = -ik\rho Re\bar{v}_1\hat{u}_1 - \mathtt{D}\hat{p}_1 + \mu(\mathscr{L}\hat{u}_1 - \frac{\hat{u}_1}{r^2}), \tag{46}$$

$$\rho Re\omega\hat{v}_1 = -\rho Re\mathtt{D}\bar{v}_1\hat{u}_1 - ik\rho Re\bar{v}_1\hat{v}_1 - ik\hat{p}_1 + \mu\mathscr{L}\hat{v}_1, \tag{47}$$

$$\mathscr{L}\hat{\phi}_1 = 0. \tag{48}$$

Boundary conditions at $r = a$ for the perturbed system are

$$\hat{u}_2 = \hat{v}_2 = \hat{\phi}_2 = 0. \tag{49}$$

At $r = b$, the boundary conditions of the perturbed system are

$$\hat{u}_1 = \hat{v}_1 = \hat{\phi}_1 = 0. \tag{50}$$

The boundary conditions at the liquid-liquid interface $r = a + h$ are projected to $r = a + 1$ by using the Taylor's expansion. The interface is perturbed to $h = 1 + \hat{\eta}\exp(ikz + \omega t)$, where $\hat{\eta}$ measures the deformation of the interface. After dropping the higher order terms, the conditions of perturbed velocities read

$$\hat{u}_2 = \hat{u}_1, \quad \hat{v}_2 + \mathtt{D}\bar{v}_2\hat{\eta} = \hat{v}_1 + \mathtt{D}\bar{v}_1\hat{\eta}. \tag{51}$$

The voltage potential conditions of the perturbed system at the interface are

$$\hat{\phi}_2 + \mathtt{D}\bar{\phi}_2\hat{\eta} = \hat{\phi}_1 + \mathtt{D}\bar{\phi}_1\hat{\eta}, \quad \mathtt{D}\hat{\phi}_2 + \mathtt{D}^2\bar{\phi}_2\hat{\eta} = \sigma(\mathtt{D}\hat{\phi}_1 + \mathtt{D}^2\bar{\phi}_1\hat{\eta}), \tag{52}$$

and note that $\mathtt{D}\bar{\phi}_2 = \sigma\mathtt{D}\bar{\phi}_1$, and $\mathtt{D}^2\bar{\phi}_2 = \sigma\mathtt{D}^2\bar{\phi}_1$.

The perturbed stress balance condition in tangential and normal direction, respectively, reads

$$[ik\hat{u} + \mathtt{D}\hat{v} + \mathtt{D}^2\bar{v}\hat{\eta}]_2 - \mu[ik\hat{u} + \mathtt{D}\hat{v} + \mathtt{D}^2\bar{v}\hat{\eta}]_1 + We[\varepsilon_2\mathtt{D}\bar{\phi}_2(ik\mathtt{D}\bar{\phi}_2\hat{\eta} + ik\hat{\phi}_2) - \varepsilon_1\mathtt{D}\bar{\phi}_1(ik\mathtt{D}\bar{\phi}_1\hat{\eta} + ik\hat{\phi}_1)] = 0, \tag{53}$$

$$- \hat{p}_2 + 2[\mathrm{D}\hat{u} - ik\mathrm{D}\bar{v}\hat{\eta}]_2 + \hat{p}_1 - 2\mu[\mathrm{D}\hat{u} - ik\mathrm{D}\bar{v}\hat{\eta}]_1$$
$$+ We[\varepsilon_2 \mathrm{D}\bar{\phi}_2(\mathrm{D}^2\bar{\phi}_2\hat{\eta} + \mathrm{D}\hat{\phi}_2) - \varepsilon_1 \mathrm{D}\bar{\phi}_1(\mathrm{D}^2\bar{\phi}_1\hat{\eta} + \mathrm{D}\hat{\phi}_1)] = \frac{1}{Ca}[\frac{\hat{\eta}}{(a+1)^2} - k^2\hat{\eta}]. \quad (54)$$

The perturbed kinematic condition is

$$\omega\hat{\eta} + ik\bar{v}_2\hat{\eta} - \hat{u}_2 = 0. \quad (55)$$

V. RESULTS AND DISCUSSION

A. Effects of the electric field

This section discusses the influences of electric field on instability of the interface theoretically. The governing equation of the perturbed electric field can be solved by Bessel's function,

$$\hat{\phi}_1 = e_1 I_0(kr) + e_2 J_0(kr), \quad \hat{\phi}_2 = e_3 I_0(kr) + e_4 J_0(kr), \quad (56)$$

in which I_0, J_0 are modified Bessel's functions of order zero, and $I'_0 = kI_1$, $J'_0 = -kJ_1$ where I_1, J_1 are modified Bessel's functions of order one. Using the boundary conditions, the coefficients are determined as follows:

$$e_1 = \frac{1}{\mathcal{P}} \frac{1-\sigma}{(a+1)[\sigma \ln \frac{a}{a+1} + \ln \frac{a+1}{b}]}\hat{\eta}, \quad (57)$$

$$e_2 = -I_0(kb)/J_0(kb)e_1, \quad (58)$$

$$e_3 = \mathcal{Q}e_1, \quad (59)$$

$$e_4 = -I_0(ka)/J_0(ka)\mathcal{Q}e_1, \quad (60)$$

with

$$\mathcal{P} = \mathcal{Q}\frac{I_0(ka+k)J_0(ka) - J_0(ka+k)I_0(ka)}{J_0(ka)} - \frac{I_0(ka+k)J_0(kb) - J_0(ka+k)I_0(kb)}{J_0(kb)}, \quad (61)$$

$$\mathcal{Q} = \sigma \frac{J_0(ka)}{J_0(kb)} \frac{I_1(ka+k)J_0(kb) + J_1(ka+a)I_0(kb)}{I_1(ka+k)J_0(ka) + J_1(ka+a)I_0(ka)}. \quad (62)$$

In the normal stress balance condition, Eq. (54), the term $[\varepsilon_2 \mathrm{D}\bar{\phi}_2\mathrm{D}^2\bar{\phi}_2 - \varepsilon_1 \mathrm{D}\bar{\phi}_1\mathrm{D}^2\bar{\phi}_1]\hat{\eta}$ is equal to $-\frac{\varepsilon_2\sigma^2-\varepsilon_1}{(a+1)^3[\sigma \ln \frac{a}{a+1}+\ln \frac{a+1}{b}]^2}\hat{\eta}$, and the other term $[\varepsilon_2 \mathrm{D}\bar{\phi}_2\mathrm{D}\hat{\phi}_2 - \varepsilon_1 \mathrm{D}\bar{\phi}_1\mathrm{D}\hat{\phi}_1] = \frac{\varepsilon_2\sigma^2-\varepsilon_1}{(a+1)[\sigma \ln \frac{a}{a+1}+\ln \frac{a+1}{b}]}\mathrm{D}\hat{\phi}_1$. According to the solution of the electric field, $\mathrm{D}\hat{\phi}_1 = k[I_1(ka+k) + I_0(kb)J_1(ka+k)/J_0(kb)]e_1$ which is modified as

$$\mathrm{D}\hat{\phi}_1 = \frac{k[I_1(ka+k) + I_0(kb)J_1(ka+k)/J_0(kb)]}{\mathcal{P}} \frac{1-\sigma}{(a+1)[\sigma \ln \frac{a}{a+1} + \ln \frac{a+1}{b}]}\hat{\eta}, \quad (63)$$

then, the effect of electric field on the interfacial stability is proportional to

$$[S\frac{(\varepsilon_2\sigma^2 - \varepsilon_1)(1-\sigma)}{(a+1)^2[\sigma \ln \frac{a}{a+1} + \ln \frac{a+1}{b}]^2} - \frac{\varepsilon_2\sigma^2 - \varepsilon_1}{(a+1)^3[\sigma \ln \frac{a}{a+1} + \ln \frac{a+1}{b}]^2}]\hat{\eta}.$$

The parameter $S = \frac{k[I_1(ka+k)+I_0(kb)J_1(ka+k)/J_0(kb)]}{\mathcal{P}}$. The value of S is found to be always positive. For small to moderate Reynolds numbers, the system is susceptible to the Plateau-Rayleigh instability and interface wave instability.[30] The former is caused by surface tension due to the azimuthal curvature; and the latter is due to viscosity stratification. The capillary and interface wave instabilities are associated with interface deformation. It is noted that, when $\sigma^2 = \varepsilon_1/\varepsilon_2$, the normal Maxwell stress becomes zero at the liquid-liquid interface.

For this two-fluid core-annular system, when

$$\sigma^2 > \varepsilon_1/\varepsilon_2 \quad and \quad \sigma < 1 - \frac{1}{S(a+1)}, \tag{64}$$

or

$$\sigma^2 < \varepsilon_1/\varepsilon_2 \quad and \quad \sigma > 1 - \frac{1}{S(a+1)}, \tag{65}$$

the electric field impedes the deformation of interface. Otherwise, it enhances the deformation of interface. This two core-annular flow system can be reduced to a bilayer system coflowing between two parallel infinite plates when the inner radius a is infinitely large, i.e., $a \to \infty$. Equations (64) and (65) agree with the results by Ozen *et al.*[15] when $a \to \infty$ and the charge relation time is fast. Ozen *et al.*[15] proposed that, for the two-fluid layer flowing between two parallel plates in a normal electric field, when $\sigma^2 > \varepsilon_1/\varepsilon_2$ and $\sigma < 1$, or $\sigma^2 < \varepsilon_1/\varepsilon_2$ and $\sigma > 1$, the electric field can stabilize the system. Otherwise, the electric field destabilizes the system. However, the criterion set by Ozen *et al.*[15] is only valid to explain the normal Maxwell stress's effect which cannot be used to explain the effect of the tangential Maxwell stress.[16] The surface charge induces a tangential Maxwell stress which has an important effect on the stability of the system. Nevertheless, for the core-annular flow system, when the instability is dominated by the capillary force, the theoretical results in Eqs. (64) and (65) can be referred as a criterion of capillary instability. When the electrical properties satisfy Eqs. (64) or (65), the electric field can impede the capillary instability. Otherwise, the electric field enhances the capillary instability. Furthermore, when the electrical properties do not satisfy Eqs. (64) or (65), the electric field always enhances the deformation of interface.

Since we are considering leaky dielectrics, free charges accumulate at the liquid-liquid interface which induces a tangential Maxwell stress qE_t(q is the surface charge density and E_t is the tangential component of $\mathbf{E}$ at the liquid-liquid interface). Viscous stress at the liquid-liquid interface is balanced by the tangential Maxwell stress. In Eq. (53), the linearized tangential Maxwell stress is

$$ik\frac{(\varepsilon_2\sigma - \varepsilon_1)}{(a+1)^2[\sigma \ln \frac{a}{a+1} + \ln \frac{a+1}{b}]^2}(1 + \mathcal{R}(1-\sigma))\hat{\eta},$$

in which, $\mathcal{R} = \frac{I_0(ka+k) - I_0(kb)J_0(ka+k)/J_0(kb)}{\mathcal{P}} < 0$. The tangential Maxwell stress is zero when $\sigma = \varepsilon_1/\varepsilon_2$. The influence of the tangential Maxwell stress on the interfacial instabilities (the capillary and interface wave instabilities) is very complex because it is coupled with the viscous stress. Particularly, when $\sigma = \varepsilon_1/\varepsilon_2 = 1$, the electric field has no influences on the system because both the normal and tangential Maxwell stress are zero in the stress balance condition.

We will examine the influences of the electric field on the interfacial instabilities in Sec. V B numerically.

B. Numerical results

This section presents the numerical results of the linear stability analysis. The eigenvalue problem was resolved by the Chebyshev collocation method. The computation domain of each layer was transformed to the Chebyshev domain $[-1, 1]$.

For the inner layer, the transformation is

$$y_2 = 2(r - a) - 1. \tag{66}$$

For the outer layer, the transformation is

$$y_1 = 2\frac{r - (a+1)}{b - (a+1)} - 1. \tag{67}$$

The solution of the perturbed system is achieved by Chebyshev polynomials,

$$[\hat{u}, \hat{v}, \hat{\phi}]_i = \sum_{j=0}^{N} [U_j, V_j, \Phi_j]_i T_j, \tag{68}$$

where $T_j = \cos(j\cos^{-1}y)$ with $y \in [-1, 1]$ is the Chebyshev polynomial.

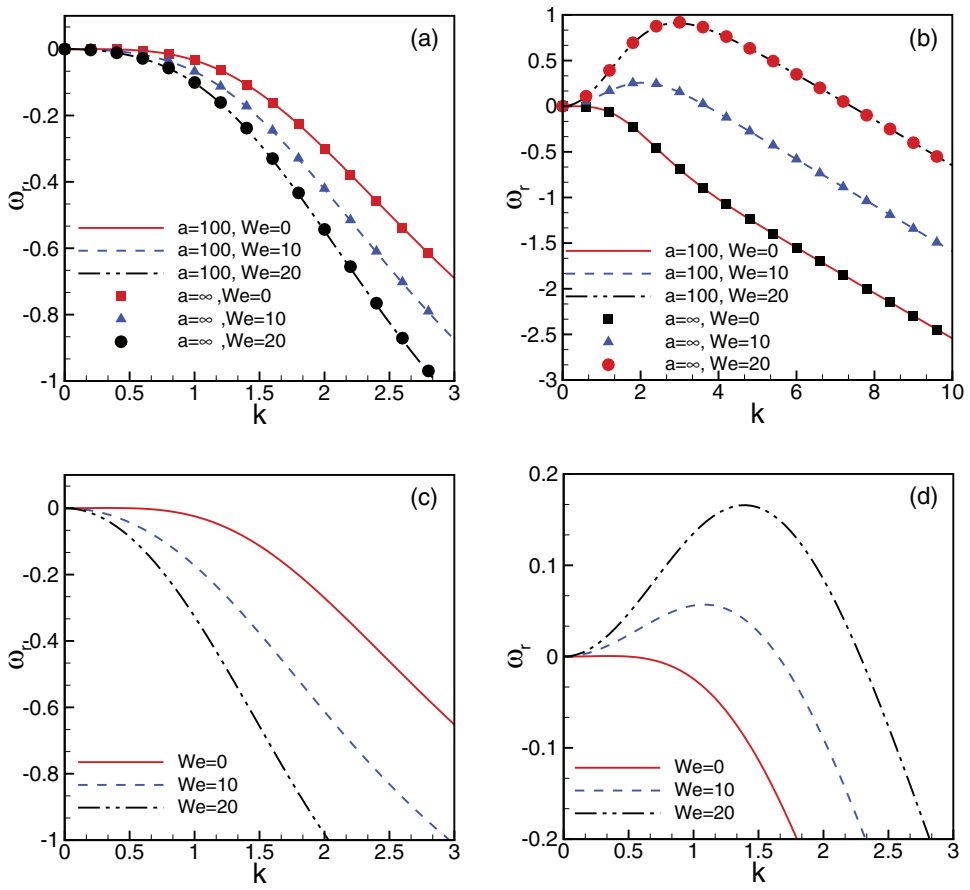

FIG. 2. Effective Growth rate versus disturbance wave number. (a) $\varepsilon_1 = 2$, $\varepsilon_2 = 10$, $\sigma = 0.5$. (b) $\varepsilon_1 = 5$, $\varepsilon_2 = 10$, $\sigma = 0.5$. (c) $\varepsilon_1 = 10$, $\varepsilon_2 = 1$, $\sigma = 1$. (d) $\varepsilon_1 = 5$, $\varepsilon_2 = 10$, $\sigma = 1$. The other parameters $Re = Ca = a = H = \rho = \mu = 1$.

As shown in Figure 2(a), when $\sigma^2 > \varepsilon_1/\varepsilon_2$ and $\sigma < 1 - \frac{1}{S(a+1)}$, the electric field impedes the capillary instability. Figure 2(b) shows that when the electric field strength increases, i.e., increasing the value of We, the effective growth rate ω_r increases indicating that the electric field is destabilizing when $\sigma^2 < \varepsilon_1/\varepsilon_2$ and $\sigma < 1 - \frac{1}{S(a+1)}$. In Figures 2(a) and 2(b), we reproduced the results by Ozen *et al.*[15] at the limiting case $a = \infty$. Figures 2(a) and 2(b) show that, when a is large, our results agree with the results of a planar system.[15] In Figure 2(c), when $\sigma^2 < \varepsilon_1/\varepsilon_2$ and $\sigma > 1 - \frac{1}{S(a+1)}$, the electric field stabilizes the system. In Figure 2(d), $\sigma^2 > \varepsilon_1/\varepsilon_2$ and $\sigma > 1 - \frac{1}{S(a+1)}$, the electric field is destabilizing.

To examine the tangential Maxwell stress on the interfacial instability, two typical values of electrical conductivity ratio is chosen, $\sigma = 0.5, 2$ and the permittivity ratio $\varepsilon = \varepsilon_1/\varepsilon_2 = \sigma^2$ so that the normal Maxwell stress vanishes in Eq. (54). Results in Figure 3 illustrate that the effect of tangential Maxwell stress on the instability is strongly influenced by the viscosity ratio. As seen in Figure 3(a), for $\sigma^2 = \varepsilon_1/\varepsilon_2 = 0.25$, $\mu = 1$, the electric field is stabilizing; when $\sigma^2 = \varepsilon_1/\varepsilon_2 = 4$, $\mu = 1$, the electric field is destabilizing as shown in Figure 3(b). When the viscosity ratio is increased to $\mu = 2$, the electric field's influence on the stability is changed. In Figure 3(c), although the input electrical properties are the same as those in Figure 3(a), the electric field is destabilizing. Furthermore, same input values of electrical properties are selected in Figure 3(d) as in Figure 3(b). It is observed that the electric field stabilizes the long-wave mode but destabilizes the short wave mode as is seen in Figure 3(d).

It is noted that both the normal and tangential Maxwell stresses either stabilize or destabilize the interface. We show that the effects of normal and tangential Maxwell stress on the perturbed

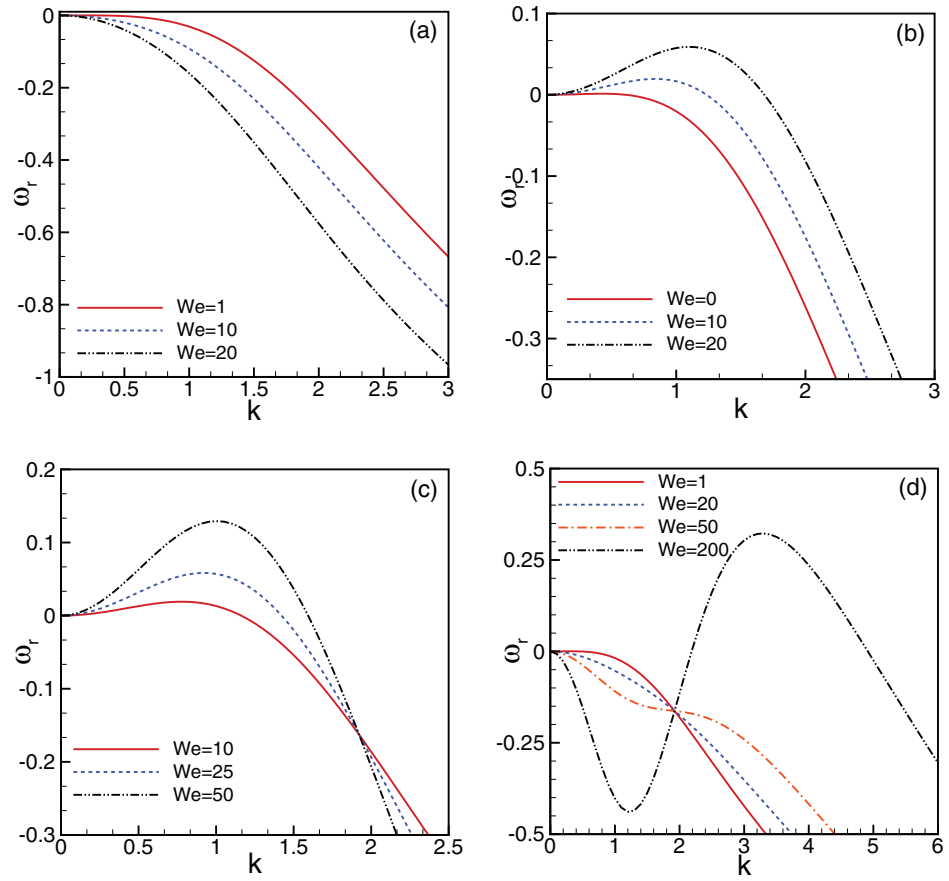

FIG. 3. The tangential Maxwell stress effect on the growth rate. (a) $\varepsilon_1 = 2.5$, $\varepsilon_2 = 10$, $\sigma = 0.5$, $\mu = 1$; (b) $\varepsilon_1 = 10$, $\varepsilon_2 = 2.5$, $\sigma = 2$, $\mu = 1$; (c) $\varepsilon_1 = 2.5$, $\varepsilon_2 = 10$, $\sigma = 0.5$, $\mu = 2$; (d) $\varepsilon_1 = 10$, $\varepsilon_2 = 2.5$, $\sigma = 2$, $\mu = 2$. The other parameters $Re = Ca = a = H = \rho = 1$.

flow field are different. Here, a streamfunction of the perturbed flow field ψ' is defined as follows:

$$u'_i = \frac{1}{r}\frac{\partial \psi'_i}{\partial z}, \quad v'_i = -\frac{1}{r}\frac{\partial \psi'_i}{\partial r}, \tag{69}$$

where $(u', v')_i$ is the velocity of the perturbed flow system.

Figure 4 illustrates the electric field's influence on flow field in the long-wave range. In Figure 4(a), tangential Maxwell stress vanishes for the input electrical properties while the normal stress destabilizes the interface. In Figure 4(b), the selected values of electrical properties are the same as those in Figure 3(b) that the tangential Maxwell destabilizes the interface and the normal Maxwell stress is zero. We observe that, the convection cells in Figure 4(a) are different from that in Figure 4(b). Since in the long-wave range, the instability is dominated by capillary forces. In Figure 4(a), convection is due to the deformation of interface caused by the capillary instability and the flow pattern will not change no matter how large the electric field is imposed; while in Figure 4(b), the tangential Maxwell stress can induce a circulation flow in each layer and the flow pattern may change with the imposed electric field because its magnitude changes with the imposed strength of electric field. The instability caused by the tangential Maxwell stress is very much like that of Marangoni effect.[31]

The effect of the dielectric permittivity on the growth rate is shown in Figure 5(a). The permittivity $\varepsilon_1 = 1$ is held fixed. The value of ε_2 is varied to study the influence of permittivity on the dispersive relation. In Figure 5(a), the selected parameters give $\sigma^2 < \varepsilon_1/\varepsilon_2$ and $\sigma < 1 - \frac{1}{S(a+1)}$. Thus, the electric field is destabilizing.

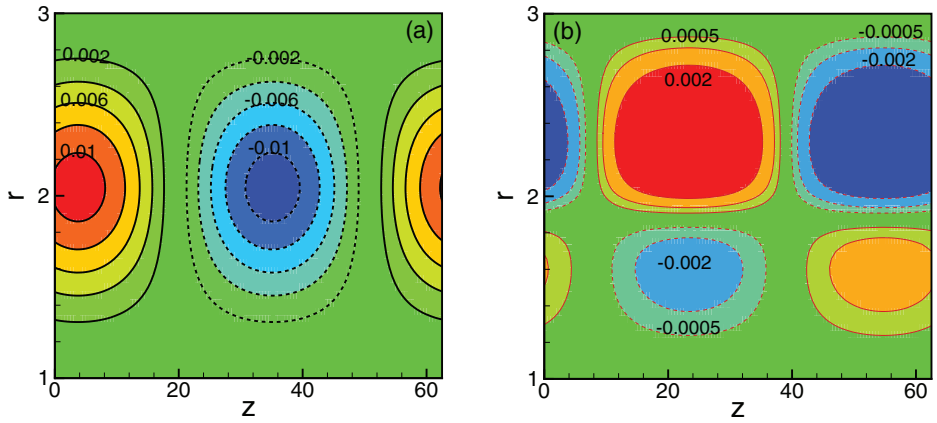

FIG. 4. Perturbed flow field plotted by the streamfunction ψ'. (a) $\varepsilon_1 = 10$, $\varepsilon_2 = 5$, $\sigma = 2$; (b) $\varepsilon_1 = 10$, $\varepsilon_2 = 2.5$, $\sigma = 2$. The other dependent parameters $Re = \rho = Ca = a = H = \mu = 1$, $We = 10$, $k = 0.1$.

The effect of the electric field on the interfacial deformation is proportional to $\sigma^2 - \varepsilon_1/\varepsilon_2 < 0$. The value of $|\sigma^2 - \varepsilon_1/\varepsilon_2|$ (the destabilizing effect of the electric field) decreases as ε_2 increases. Therefore, when ε_2 increases, the effective growth rate decreases. Figure 5(b) presents the influence of the electrical conductivity ratio $\sigma = \sigma_1/\sigma_2$ on the effective growth rate and indicates the growth rate decreases with increasing the conductivity ratio. For the selected parameters, the value of $|\sigma^2 - \varepsilon_1/\varepsilon_2|$ decreases as σ increases. As a result, the enhancement of the electric field on the deformation of interface decreases as σ increases. Therefore, the growth rate decreases as σ increases. Here, we define (ω_m, k_m) as the effective growth rate and wave number of the most unstable perturbation as shown in Figure 5(b). The most unstable perturbation is the major cause of interfacial instabilities, and its wave length characterizes the size of liquid droplets that is formed due to the interface's rupture.[12]

Influence of the radius of the inner cylinder on the growth rate is shown in Figure 6(a). It should be noted that when $k < \frac{1}{a+1}$, the destabilizing effect of surface tension dominates its stabilizing effect. When $k < \frac{1}{a+1}$, reducing the inner radius a would increase the destabilizing effect.[20] Thus, the system would be more unstable when a becomes smaller. Similar results are shown in Figure 6(b), in which, the electrical Weber number is fixed at zero so as to investigate the influences

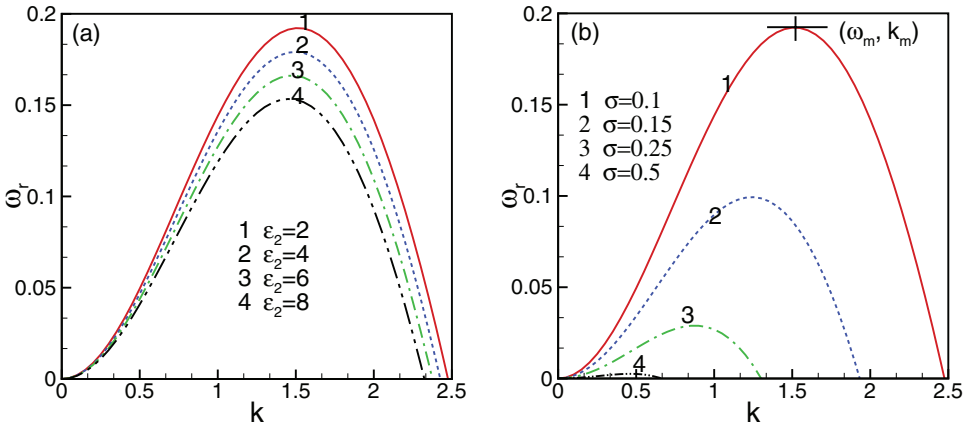

FIG. 5. (a) Electrical permittivity on the effective growth rate. The dependent parameters $Re = \rho = Ca = We = a = 1$, $H = 0.5$, $\sigma = \mu = 0.1$. (b) Electrical conductivity ratio on the effective growth rate. The dependent parameters $Re = \rho = Ca = We = a = 1$, $H = 0.5$, $\mu = 0.1$, $\varepsilon_1 = 1$, $\varepsilon_2 = 2$.

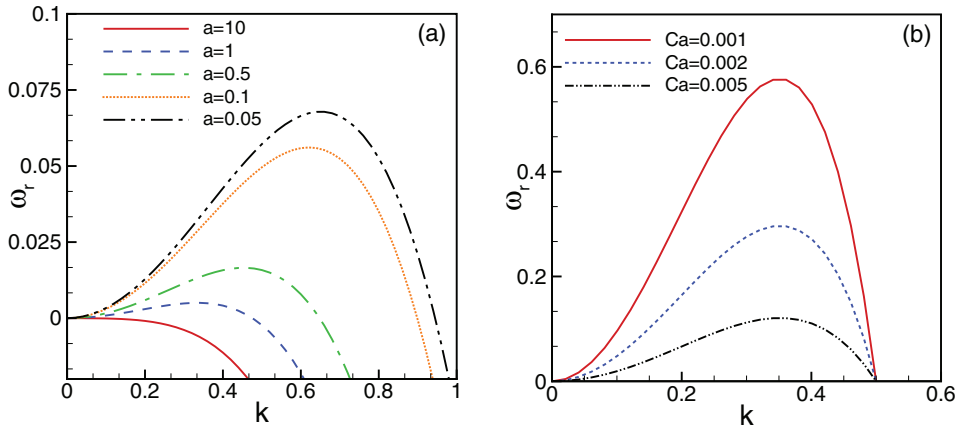

FIG. 6. (a) Inner radius of the duct on the effective growth rate. The dependent parameters are $\varepsilon_1 = 1$, $\varepsilon_2 = 10$, $\sigma = 0.5$, $Ca = 0.1$, $We = a = H = Re = \rho = \mu = 1$. (b) Capillary number Ca on the effective growth rate. The depending parameter $Re = a = H = \rho = \mu = 1$, $We = 0$.

of surface tension. It is obvious that the capillary force is destabilizing the system in the long wave range due to the azimuthal curvature.

Influence of thickness of the outer layer H is investigated as shown in Figure 7. It is observed that the growth rate decreases with increasing the thickness of the outer layer. First, the total fluid mass increases when the thickness of the outer liquid layer increases. Second, the electric strength reduces as the radius b increases.[23] Therefore, the effective growth rate decreases with increasing the thickness of the outer layer.

We further investigate the influences of the viscosity ratio μ. Results are shown in Figure 8. Figure 8(a) shows that the effective growth rate ω_r increases with increasing μ, while in Figure 8(b), the effective growth rate ω_r decreases with increasing μ. Results in Figure 8 show the viscosity either destabilizes or stabilizes the system. The destabilizing effect is due to viscosity stratification.[30] However, the viscous dissipation of the system increases for a larger μ. As a result, the system becomes more stable as shown in Figure 8(b).

We are interested in investigating how large the electric field should be imposed, such that it can impede the capillary instability. To study the problem, we plot the marginal curve in $We - k$ plane in Figure 9(a), in which, the electrical properties are chosen that the electric field can impede the capillary instability. The viscosity ratio is $\mu = 5$ and the Reynolds number is fixed at $Re = 1$.

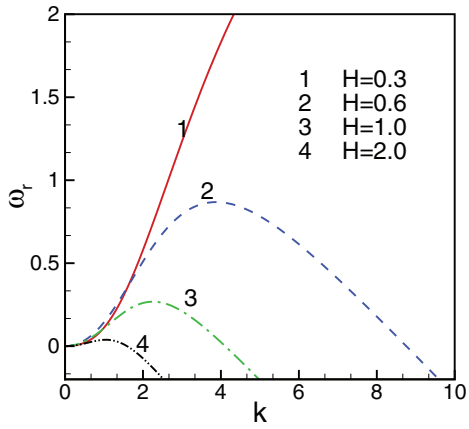

FIG. 7. Thickness ratio on the effective growth rate. The dependent parameters $Re = \rho = \mu = Ca = We = a = 1$, $\varepsilon_1 = 5$, $\varepsilon_2 = 10$, $\sigma = 0.1$.

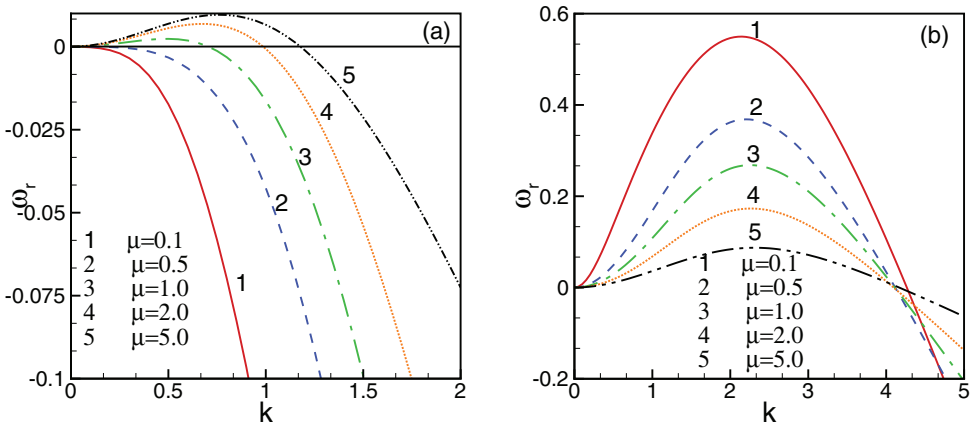

FIG. 8. Viscosity ratio on the effective growth rate. (a) $\varepsilon_1 = 5$, $\varepsilon_2 = 10$, $\sigma = 1$. (b) $\varepsilon_1 = 5$, $\varepsilon_2 = 10$, $\sigma = 0.1$. The other parameters $Re = \rho = Ca = We = 1$, $a = 1$, $b = a + 2$.

The marginal stability curves in Figure 9(a) shows that the unstable region enlarges and the critical Weber number We_c increases as the conductivity ratio increases which indicates that a larger electric field should be imposed to stabilize the interface for a larger conductivity ratio. It is obvious that the capillary instability can be stabilized by an external electric field since a stable region exists when We exceeds its critical value. However, when $\sigma = 4$, it is observed that these is no such critical Weber number since the electric field enhances the instability for the input values of electrical properties σ, ε_1, and ε_2. As is seen in Figure 9(b), the critical electrical Weber number increases with σ and no critical electrical Weber number is found by us when $\sigma \approx 3.9$. It is found that there is a critical electrical Weber number when $\sigma = 3.7(\sigma^2 > \varepsilon_1/\varepsilon_2)$ and the electric field has a stabilizing effect that can impede the capillary instability, although the normal Maxwell stress enhances the capillary instability($\sigma^2 > \varepsilon_1/\varepsilon_2$). Therefore, we conclude that, the stabilizing effect of the electric field is due to the tangential Maxwell stress.

We further fix the value of conductivity ratio, but vary the permittivity ratio $\varepsilon_1/\varepsilon_2$ to investigate the electric filed's influence on the marginal curves. Here, to simplify the discussion, the conductivity ratio is fixed at $\sigma = 1$ and the permittivity $\varepsilon_2 = 10$. The value of ε_1 is varied from $\varepsilon_1 = 1$ to $\varepsilon_1 = 20$. As seen in Figure 10(a), when $\varepsilon_1 \leq 10$, there is no critical electrical Weber number. The marginal curve does not depend on We when $\varepsilon_1 = 10$ due to the absence of Maxwell stress. The electric field can stabilize the interface with increasing the value of ε_1. For instance, $\varepsilon_1 = 10.5$,

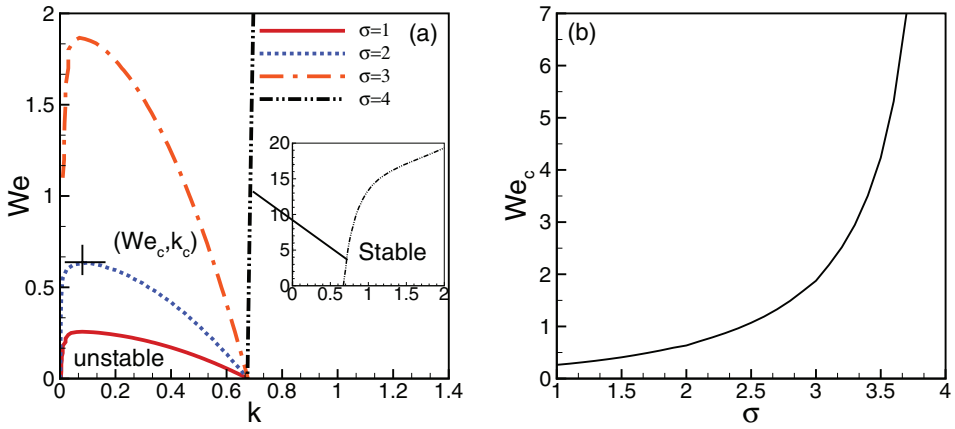

FIG. 9. (a) Marginal stability curve $We - k$. (b) The critical electrical Weber number versus the conductivity ratio. The depending parameters are $\varepsilon_1 = 10$, $\varepsilon_2 = 1$, $Re = \rho = Ca = a = H = 1$, $\mu = 5$.

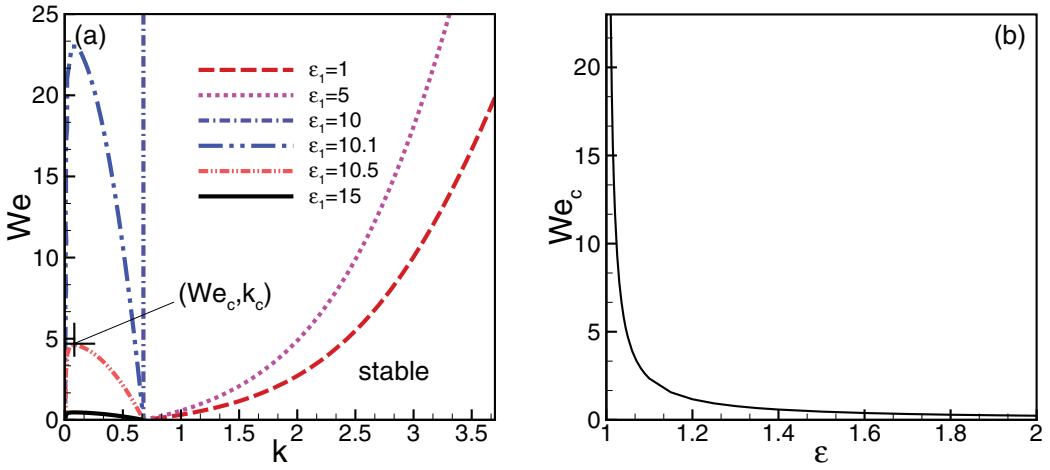

FIG. 10. (a) Marginal stability curve $We - k$. (b) The critical electrical Weber number versus the permittivity ratio $\varepsilon = \varepsilon_1/\varepsilon_2$. The depending parameters are $\varepsilon_2 = 10$, $Re = \sigma = \rho = Ca = a = H = 1$, $\mu = 5$.

when We is larger than We_c, the capillary instability is completely impeded. As the value of ε_1 increases, the electric field's suppression on the capillary instability becomes more significant as seen in Figure 10(a). This phenomenon agrees with our analysis in the above section that the electric field impedes the capillary instability when $\sigma^2 < \varepsilon_1/\varepsilon_2$ and $\sigma > 1 - \frac{1}{S(a+1)}$. In Figure 10(b), we plot the critical electrical Weber number We_c against the permittivity ratio $\varepsilon_1/\varepsilon_2$. The critical electrical Weber number is observed to decrease with increasing ε.

We examine the influence of Re on the capillary mode and results are shown in Figures 11(a) and 11(b). It is found that the larger Re the smaller is the growth rate in Figure 11(a). The value of Re can be increased through increasing V_I(the velocity at the interface). The interfacial shear effect will be enhanced as Re increases. Dijkstra indicated that the interfacial shear can stabilize the capillary breakup phenomenon.[30] In this paper, the effective growth rate decreases with increasing Re, which also indicates that the interfacial shear impedes the capillary instability. To exemplify the influences of Re on the capillary instability, we plot the contour lines of growth rate in $Re - k$ plane as shown in Figure 11(b). First, we fix the wave number k, for instance, $k = 2.5$. Then, we observe that the growth rate decreases as Re increases. The marginal curve corresponding to the zero growth rate in Figure 11(b) bends leftward which indicates that the capillary instability is stabilized by interfacial shear.

The interface may be unstable due to viscosity stratification (interface wave mode) when Re is moderate.[30] Furthermore, we plot the marginal curves in the $Re - k$ plane to examine the electric field's influence on the interface wave mode due to viscosity stratification across the interface. Results are shown in Figures 11(c) and 11(d). In order to discuss the electric field's influences on the interface wave mode, the capillary number Ca is replaced by Re/J where $J = \gamma h_0 \rho_2/\mu_2{}^2$. The surface tension number J is fixed at zero so that the capillary instability due to the azimuthal curvature vanishes. The input values in Figure 11(c) are chosen with reference from Dijkstra,[30] but the values of radii a, b are slightly different. In our case, $a = 0.1$. While in the work of Dijkstra,[30] $a \approx 0.11$. When $We = 0$, we observe that we can produce a similar marginal curve as that by Dijkstra.[30] When $We > 0$, for the selected input values of electrical properties in Figure 11(c), the normal Maxwell stress is zero. We observe that the marginal curve moves leftward as We increases, which indicates that the tangential Maxwell stress enhances the interface wave instability since the stable region in the $Re - k$ plane becomes smaller. In Figure 11(d), the electrical properties are fixed at $\varepsilon_1 = 10$, $\varepsilon_2 = 5$, $\sigma = 2$, so that the tangential component of Maxwell stress is zero in Eq. (53). In Figure 11(d), we observe that the electric field enhances the interface wave mode since the stable region in the $Re - k$ plane shrinks as We increases. Results in Figure 11(d) indicate that the electric field enhances the deformation of the interface($\sigma^2 > \varepsilon_1/\varepsilon_2$ and $\sigma > 1 - \frac{1}{S(a+1)}$), thus destabilizes the system.

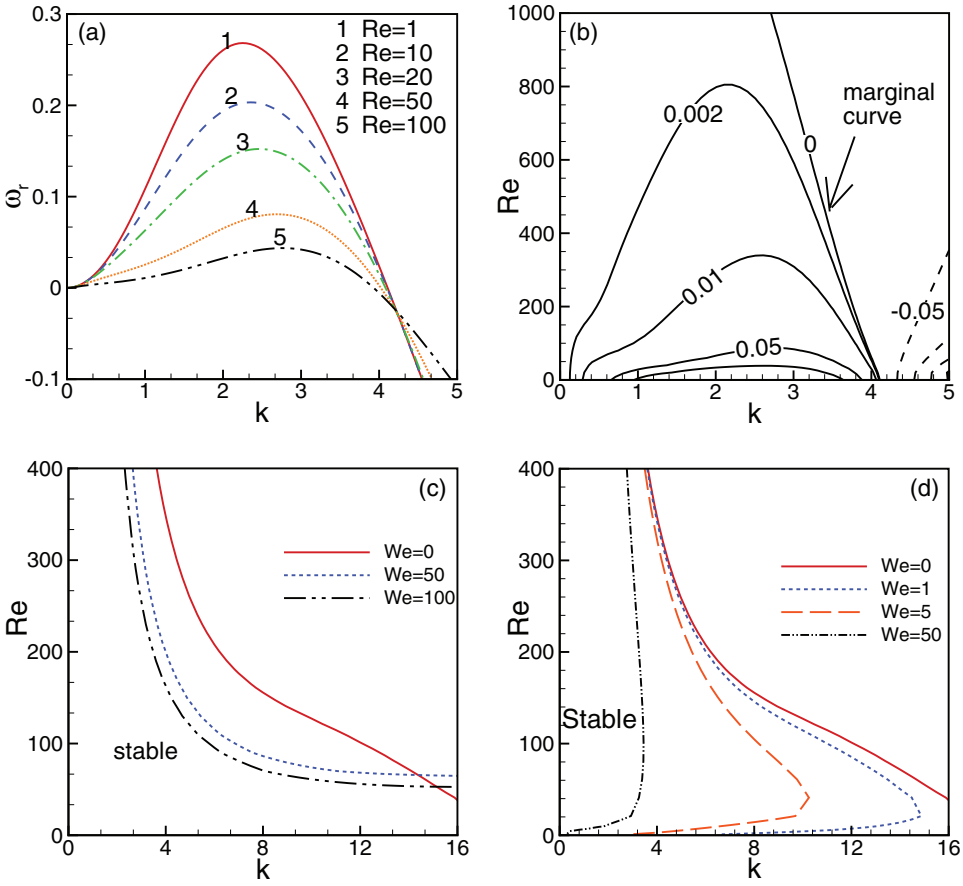

FIG. 11. (a) The Reynolds number Re on the effective growth rate. The dependent parameters $\rho = \mu = Ca = We = a = H = 1$, $\varepsilon_1 = 5$, $\varepsilon_2 = 10$, $\sigma = 0.1$. (b) The contour plot of growth rate in $Re - k$ plane. The dependent parameters are the same as Figure 11(a). (c) The marginal stability curves for interface wave mode. The dependent parameters $\rho = 1$, $a = 0.1$, $H = 0.1$, $\mu = 0.5$, $J = 0$, $\varepsilon_1 = 10$, $\varepsilon_2 = 2.5$, $\sigma = 2$. (d) The marginal stability curves for interface wave mode. The dependent parameters $\rho = 1$, $a = 0.1$, $H = 0.1$, $\mu = 0.5$, $J = 0$, $\varepsilon_1 = 10$, $\varepsilon_2 = 5$, $\sigma = 2$.

We are interested in the question: can the electric field impede the interface wave instability in Figures 11(c) and 11(d) as well as the capillary instability? The condition $\sigma = \varepsilon_1/\varepsilon_2$ is considered so that no tangential Maxwell stress is present on the interface. According to Eq. (65), the condition that the electric field can stabilize the interface requires

$$1 - \frac{1}{S(a+1)} < \sigma < \sqrt{\varepsilon_1/\varepsilon_2}, \tag{70}$$

and $\sigma = \varepsilon_1/\varepsilon_2$ implies that $\sigma < 1$. When $a \to \infty$, these is no such condition in Eq. (70) that the electric field can impede the interface wave mode when $\sigma = \varepsilon$. The expression of S varies with the wave number k, the radii a, b, and the conductivity ratio σ. Here, the radii are fixed at $a = 0.1$, $b = 1.2$. In the range of wave number $k \in [0, 16]$, we are looking for a sufficient condition for σ that the electric field can impede the interfacial instabilities(capillary and interface wave instabilities) and modify Eq. (70) as

$$max\{1 - \frac{1}{S(a+1)}\} < \sigma < 1. \tag{71}$$

Such a range of σ in Eq. (71) does exist, which is shown in Figure 12(a) as indicated by "stabilizing region." In this region, the electric field can stabilize the interfacial instabilities because it impedes the deformation of interface. Numerical verification of Eq. (71) is shown in Figure 12(b). The surface tension number in Figure 12(b) is fixed at $J = 10$ which changes the topology of the marginal curve

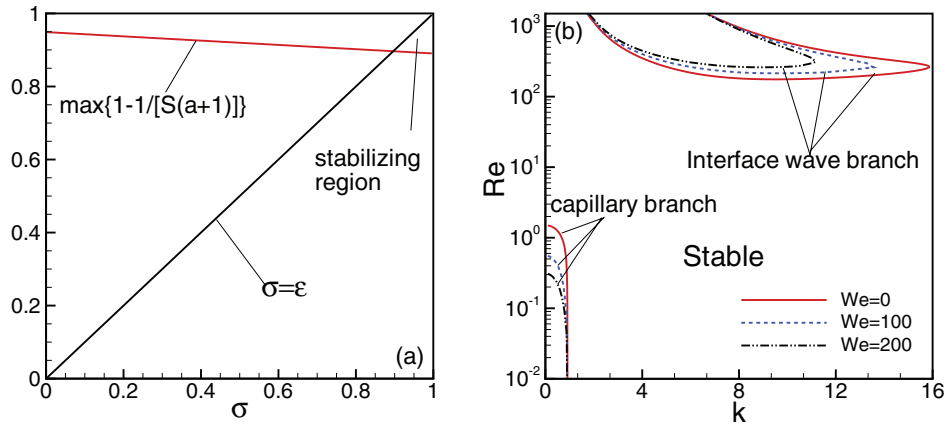

FIG. 12. (a) The conductivity ratio σ versus the maximum value of $1 - \frac{1}{S(a+1)}$ in wavenumber range [0, 16]. (b) The marginal stability curves for interface wave mode. The dependent parameters $\rho = 1$, $a = 0.1$, $H = 0.1$, $\mu = 0.5$, $J = 10$, $\varepsilon_1 = 9$, $\varepsilon_2 = 10$, $\sigma = 0.9$.

of the interface wave branch. The conductivity ratio and permittivity ratio are $\sigma = \varepsilon = 0.9$. The interface wave branch moves upward while the capillary branch moves downward as We increases, which demonstrates that the electric field can impede the capillary the interface wave instabilities. Apart from that, in Figure 12(b), it is also observed that the interfacial shear can suppress the capillary instability.

We investigate the destabilizing effect of the electric field on the interface because liquid mixing in micro-scale channels is of particular importance in industry. The Re number is usually very small in micro-scale flow systems, typically $Re = O(1)$. Therefore, in the following discussion, Re is fixed at $Re = 1$.

The electrical Weber number We is plotted against ω_m and k_m in Figure 13. It is observed that, a larger We is describing a larger ω_m and k_m. It indicates that, when the input parameters $\sigma^2 < \varepsilon_1/\varepsilon_2$ and $\sigma < 1 - \frac{1}{S(a+1)}$, the electric field enhances the deformation of the interface, thus destabilizing the system. Figure 14 shows the conductivity ratio's influence on ω_m and k_m. The magnitude of electric field's effect on the deformation of interface is proportional to $|\sigma^2 - \varepsilon_1/\varepsilon_2|$. When $\sigma < 1 - \frac{1}{S(a+1)}$, and $\sigma^2 < \varepsilon_1/\varepsilon_2$, the interfacial deformation is enhanced by the electric field and the electric field plays a destabilizing role in the system. The value of $|\sigma^2 - \varepsilon_1/\varepsilon_2|$ decreases with increasing σ. As a result,

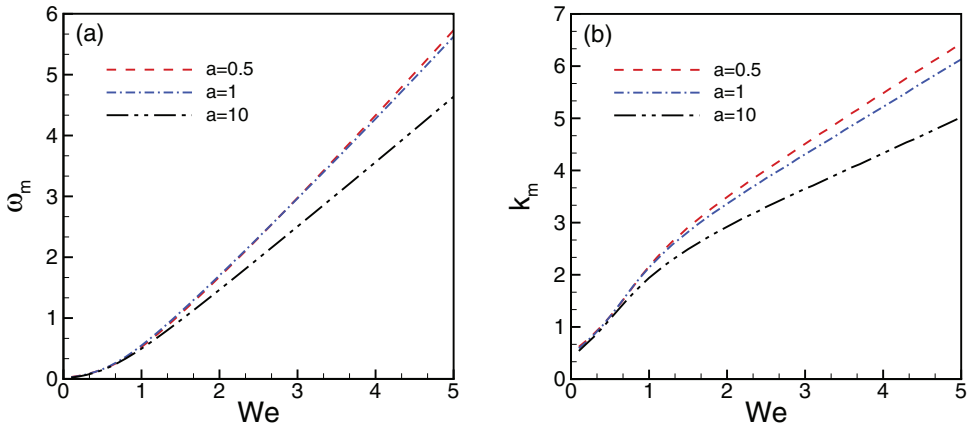

FIG. 13. The electrical Weber number on the maximum growth rate and wave number. The dependent parameters $Re = \rho = Ca = H = 1$, $\mu = \sigma = 0.1$, $\varepsilon_1 = 5$, $\varepsilon_2 = 10$.

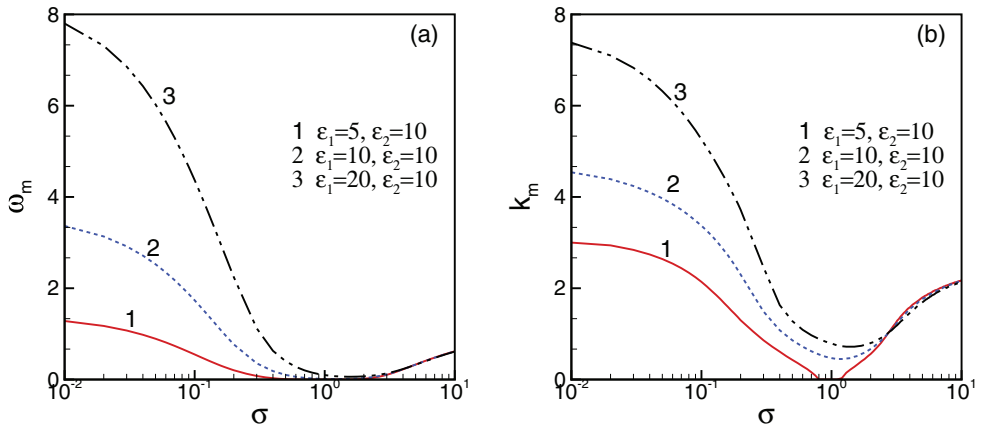

FIG. 14. The electrical conductivity ratio on the maximum growth rate and wave number. The dependent parameters $Re = \rho = Ca = H = 1 = We = a = 1$, $\mu = 0.1$.

the enhancement of electric field on the interfacial deformation reduces. Therefore, both the maximum growth rate ω_m and maximum wave number k_m decrease. With the increase in σ, the electric field may stabilize the system, i.e., $\omega_m \leq 0$. This can be seen from the stable region for $\varepsilon_1 = 5$ and $\varepsilon_2 = 10$. When $\sigma^2 > \varepsilon_1/\varepsilon_2$ and $\sigma > 1 - \frac{1}{S(a+1)}$, the electric field destabilizes the system, and the value of $|\sigma^2 - \varepsilon_1/\varepsilon_2|$ becomes larger as σ increases. As a result, the system becomes more unstable when σ increases. It is observed that, when σ is small and $\sigma^2 < \varepsilon_1/\varepsilon_2$, ω_m and k_m increases as the value of $\varepsilon = \varepsilon_1/\varepsilon_2$ increases. This is because the value of $|\sigma^2 - \varepsilon|$ increases with increasing ε when $\sigma^2 < \varepsilon$, and the destabilizing effect of the electric field is enhanced. When $\sigma^2 > \varepsilon$ and $\sigma > 1 - \frac{1}{S(a+1)}$, the value of $\sigma^2 - \varepsilon$ reduces with increasing ε. Thus the maximum growth rate decreases. However, because the selected input values of (ε_1, ε_2) are chosen that $\sigma^2 \gg \varepsilon$, ε does not have significant influences on the growth rate and wave number when $\sigma^2 > \varepsilon$ and $\sigma > 1 - \frac{1}{S(a+1)}$, although it is found that the maximum growth rate is slightly decreased as shown in Figure 14. The influence of viscosity ratio μ on ω_m and k_m are plotted in Figure 15. For the selected input parameters, the maximum growth rate ω_m decreases with increasing the viscosity ratio μ due to the viscous dissipation. Influence of viscosity ratio μ on the maximum wave number k_m is not significant when μ is large. It is observed that when μ is very small, k_m decreases initially, then increases. This phenomenon implies that the unstable mode changes. Figure 16 shows that the perturbed flow field is stronger in the outer layer when $\mu = 0.1$, while it is stronger in the inner layer when $\mu = 4$. Results in

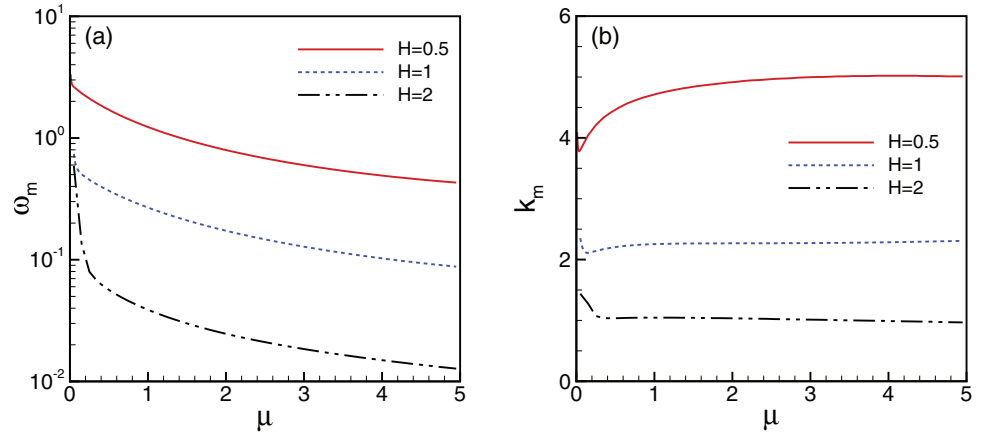

FIG. 15. The viscosity ratio on the maximum growth rate and wave number. The dependent parameters $Re = \rho = Ca = We = a = 1$, $\sigma = 0.1$, $\varepsilon_1 = 5$, $\varepsilon_2 = 10$.

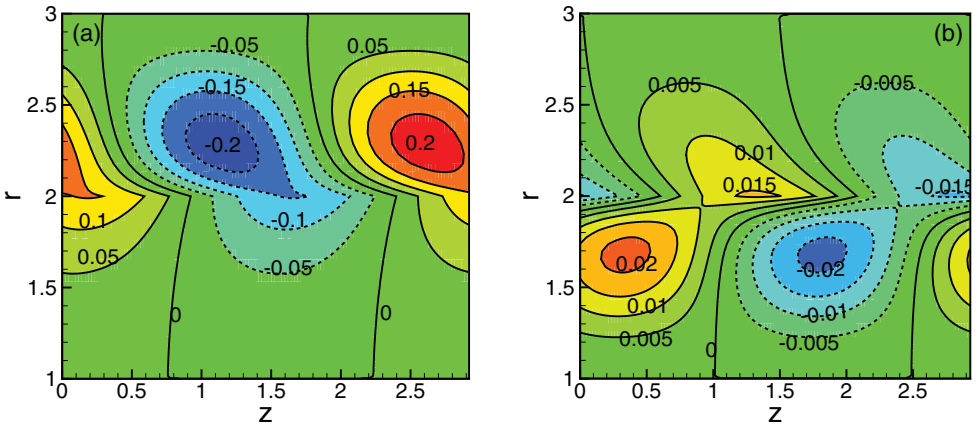

FIG. 16. Perturbed flow field plotted by the streamfunction ψ'. The dependent parameters $Re = \rho = Ca = We = a = H = 1$, $\sigma = 0.1$, $\varepsilon_1 = 5$, $\varepsilon_2 = 10$. (a) $\mu = 0.1$, $k = 2.13$; (b) $\mu = 4$, $k = 2.13$.

Figure 16 indicate that for small μ, instability is dominated by the outer layer, while for large μ, instability is dominated by the inner layer. Physically, the viscous dissipation effect is associated with the fluid viscosity. The viscous dissipation effect is stronger in the inner layer for small viscosity ratio, while it is stronger in the outer layer for large viscosity ratio. As a result, increasing μ shifts the domination of instability from the outer layer to the inner layer. Apart from that, results in Figure 15 show that the larger thickness ratio the smaller are ω_m and k_m.

VI. CONCLUSION

This paper discussed the influences of radial electric field on the interfacial instabilities of a two-fluid pressure-driven flow in an annulus duct. The two-dimensional hydrodynamical problem was considered in this paper and the normal mode analysis was carried out to study the temporal stability problem. Results of the linear stability analysis showed that, depending on the ratios of electrical properties (the electrical permittivity ratio and electrical conductivity ratio between the outer layer and inner layer), the electric field can either stabilize or destabilize the system. Both theoretical analysis and numerical studies were carried out. It was found that an external electric field can completely impede the capillary instability. Linear stability analysis showed that the system can be stabilized by increasing the inner radius of the duct or the thickness of the outer layer. It was found that viscosity had dual effects on the stability of this system. The viscosity stratification may cause instability in this system, while the viscous dissipation effect had a stabilizing effect. The Reynolds number on the stability was investigated and we found that the capillary instability could be suppressed by the interfacial shear. Apart from that, it was observed that, electric field can either stabilize or destabilize the interface wave instability due to viscosity stratification which was dependent of the electrical properties. Furthermore, a range of electrical properties were found that the electric field can suppress the capillary instability as well as the interface wave instability.

Further investigations of the input parameters on the effective growth rate and the wave number of the most unstable perturbation were conducted. In this paper, it was found that the effective growth rate and wave number depended on the strength of the electric field and the electrical permittivities and conductivities. The viscosity ratio's effect on the growth rate and wave number of the most unstable disturbance was investigated. It was found that, for selected input parameters, the instability of the system was dominated by the outer layer when the viscosity ratio was small; for large viscosity ratio, instability was dominated by the inner layer.

ACKNOWLEDGMENTS

The authors gratefully acknowledge research support from the Singapore Ministry of Education Academic Research Fund Tier 2 research grant MOE2011-T2-1-036. The authors also gratefully

acknowledge the referees for their many helpful comments. Ding Zijing thanks Mr. Sabnavis Bindumadhav for his suggestions.

[1] E. Georgiou, D. T. Papageorgiou, C. Maldarelli, and D. S. Rumschiltzki, "The double layer-capillary stability of an annular electrolyte fluid surrounding a dielectric-fluid core in a tube," J. Fluid Mech. **226**, 149–174 (1991).
[2] D. T. Conroy, R. V. Craster, O. K. Matar, and D. T. Papageorgiou, "Dynamics and stability of an annular electrolyte film," J. Fluid Mech. **656**, 481–506 (2010).
[3] M. G. Blyth, "Effect of an electric field on the stability of contaminated film flow down an inclined plane," J. Fluid Mech. **595**, 221–237 (2008).
[4] Q. M. Wang, S. Mählmann, and D. T. Papageorgiou, "Dynamics of liquid jets and threads under the action of radial electric fields: Microthread formation and touchdown singularities," Phys. Fluids **21**, 032109 (2009).
[5] B. Uma and R. Usha, "Electrified film on a porous inclined plane: Dynamics and stability," Phys. Rev. E **82**, 016305 (2010).
[6] G. I. Taylor, "Studies in electrohydrodynamics. I. The circulation produced in a drop by an electric field," Proc. R. Soc. London, Ser. A **291**, 159–166 (1966).
[7] J. Melcher and W. Schwartz, "Interfacial relaxation overstability in a tangential electric field," Phys. Fluids **11**, 2604–2616 (1968).
[8] J. Melcher and C. Smith, "Electrohydrodynamic charge relaxation and interfacial perpendicular-field instability," Phys. Fluids **12**, 778–790 (1969).
[9] D. A. Saville, "Electrohydrodynamics: The Taylor-Melcher leaky dielectric model," Annu. Rev. Fluid Mech. **29**, 27–64 (1997).
[10] H. Lin, B. D. Storey, M. H. Oddy, C. H. Chen, and J. G. Santiago, "Instability of electrokinetic microchannel flows with conductivity gradients," Phys. Fluids **16**, 1922–1935 (2004).
[11] J. D. Zahn and V. Reddy, "Two phase micromixing and analysis using electrohydrodynamic instabilities," Microfluid. Nanofluid. **2**, 399–415 (2006).
[12] O. Ozen, N. Aubry, D. T. Papageorgiou, and P. G. Petropoulos, "Monodisperse drop formation in square microchannels," Phys. Rev. Lett. **96**, 144501 (2006).
[13] K. Abdella and H. Rasmussen, "Electrohydrodynamic instability of two superposed fluids in normal electric fields," J. Comput. Appl. Math. **78**, 33–61 (1997).
[14] V. Shankar and A. Sharma, "Instability of the interface between thin fluid films subjected to electric fields," J. Colloid Interface Sci. **274**, 294–308 (2004).
[15] O. Ozen, N. Aubry, D. T. Papageorgiou, and P. G. Petropoulos, "Electrohydrodynamic linear stability of two immiscible fluids in channel flow," Electrochim. Acta **51**, 5316–5323 (2006).
[16] F. Li, O. Ozen, N. Aubry, D. T. Papageorgiou, and P. G. Petropoulos, "Linear stability of a two-fluid interface for electrohydrodynamic mixing in a channel," J. Fluid Mech. **583**, 347–377 (2007).
[17] R. H. Magarvey and L. E. Outhouse, "Note on the break-up of a charged liquid jet," J. Fluid Mech. **13**, 151–157 (1962).
[18] G. Artana, G. Touchard, and H. Romat, "Absolute and convective instabilities in an electrified jet," J. Electrost. **40–41**, 33–38 (1997).
[19] G. Artana, H. Romat, and G. Touchard, "Theoretical analysis of linear stability of electrified jets flowing at high velocity inside a coaxial electrode," J. Electrost. **43**, 83–100 (1998).
[20] Lord Rayleigh, "On the capillary phenomena of jets," Proc. R. Soc. London **29**, 71–97 (1879).
[21] C. L. Burcham and D. A. Saville, "Electrohydrodynamic stability: Taylor-Melcher theory for a liquid bridge suspended in a dielectric gas," J. Fluid Mech. **452**, 163–187 (2002).
[22] F. Li, X. Yin, and X. Yin, "Instability of a viscous coflowing jet in a radial electric field," J. Fluid Mech. **596**, 285–311 (2008).
[23] J. M. López-Herrera, P. Riesco-Chueca, and A. M. Gañón-Calvo, "Linear stability analysis of axisymmetric perturbations in imperfectly conducting liquid jets," Phys. Fluids **17**, 034106 (2005).
[24] Q. M. Wang, "Breakup of a poorly conducting liquid thread subject to a radial electric field at zero Reynolds number," Phys. Fluids **24**, 102102 (2012).
[25] A. Wray, O. Matar, and D. T. Papageorgiou, "Nonlinear waves in electrified viscous film flow down a vertical cylinder," IMA J. Appl. Math. **77**, 430–440 (2012).
[26] C. S. Yih, "Instability due to viscosity stratification," J. Fluid Mech. **27**, 337–352 (1967).
[27] L. Preziosi, K. P. Chen, and D. D. Joseph, "Lubricated pipelining: Stability of core-annular flow," J. Fluid Mech. **201**, 323–356 (1989).
[28] D. D. Joseph, R. Bai, K. P. Chen, and Y. Y. Renardy, "Core-annular flows," Annu. Rev. Fluid Mech. **29**, 65–90 (1997).
[29] B. Selvam, S. Merk, R. Govindarajan, and E. Meiburg, "Stability of miscible core¨-cannular flows with viscosity stratification," J. Fluid Mech. **592**, 23–49 (2007).
[30] H. A. Dijkstra, "The coupling of interfacial instabilities and the stabilization of two-layer annular flows," Phys. Fluids A **4**, 1915–1928 (1992).
[31] R. V. Birikh, V. A. Briskman, V. G. Velarde, and J. C. Legros, *Liquid Interfacial Systems: Oscillations and Instability* (CRC Press, New York, 2003).